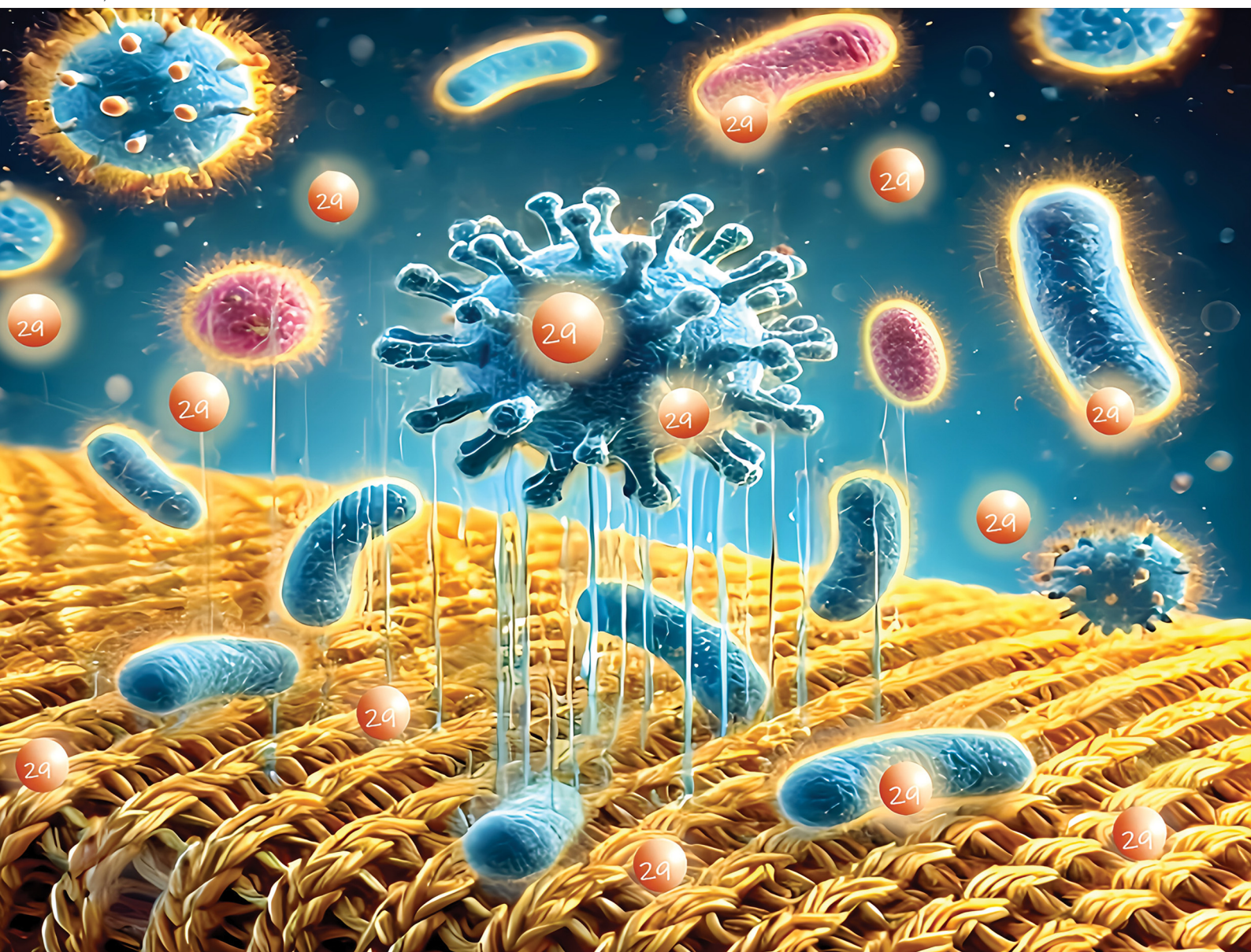


# Materials Advances

Volume 6  
Number 8  
21 April 2025  
Pages 2451–2704

[rsc.li/materials-advances](https://rsc.li/materials-advances)




ISSN 2633-5409

## PAPER

Chia-Ching Wu *et al.*  
Industrially compatible manufacturing process of  
wash-durable antimicrobial textiles using cuprous  
oxide–polymer composites

## PAPER

[View Article Online](#)  
[View Journal](#) | [View Issue](#)Cite this: *Mater. Adv.*, 2025,  
6, 2507Industrially compatible manufacturing process of  
wash-durable antimicrobial textiles using cuprous  
oxide–polymer composites†Hung-Tung Chen,<sup>a</sup> Ming-Cai Huang,<sup>b</sup> Yi-Ying Chiang,<sup>b</sup> Yong Chang<sup>b</sup> and  
Chia-Ching Wu  <sup>★a</sup>

Developing textiles with antibacterial and antiviral properties and excellent wash resistance can be a promising approach to combat multidrug-resistant bacteria, the influenza virus, and SARS-CoV-2, which are the major causes of nosocomial infections. Herein, an innovative method was developed to dope cuprous oxide nanoparticles (Cu<sub>2</sub>O NPs) possessing antimicrobial properties into raw fiber materials, thus leading to the formation of Cu<sub>2</sub>O NP-embedded masterbatches and then textiles. The textiles fabricated using the Cu<sub>2</sub>O NP-embedded masterbatches exhibited excellent antimicrobial activity (>5.21; Japanese Industrial Standard L 1902:2015) against Gram-positive and Gram-negative bacteria and *Candida albicans*, and their antimicrobial activity slightly decreased by less than 5.9% after 50 washes. Thus, the Cu<sub>2</sub>O NP-embedded textiles can effectively inhibit the growth of viruses and improve the efficacy of medical treatment. Our approach overcomes the drawback of the current techniques used for the post-processing of Cu<sub>2</sub>O NP-related antimicrobial agents for textiles. In addition, Cu<sub>2</sub>O NPs can be embedded into various raw materials used in the production of fabrics, such as polypropylene and polyethylene terephthalate, employing the developed technique. Furthermore, the developed approach can be readily commercialized.

Received 29th July 2024,  
Accepted 8th February 2025

DOI: 10.1039/d4ma00650j

[rsc.li/materials-advances](https://rsc.li/materials-advances)

## Introduction

Currently, textiles are widely used in various fields for multiple purposes. The textile industry has undergone significant advancements driven by technological innovation and increased environmental awareness. However, its primary goal remains to enhance human life. Consequently, textiles serve functions beyond protection. For instance, water-resistant jackets with high breathability can be both lightweight and warm.<sup>1</sup> Smart textiles integrate electronic components and sensing technologies to monitor physiological data.<sup>2</sup> Self-cleaning textiles, a type of functional material, can remove stains and odors without traditional washing.<sup>3</sup> Moreover, textiles made from recycled polyester fibers, such as those extracted from plastic bottles, contribute to environmental sustainability.<sup>4</sup>

Since the outbreak of the COVID-19 pandemic, which triggered a global health crisis, national economies have been severely impacted, and public health systems have been strained. During this period, antimicrobial textiles garnered widespread attention and substantial research investment due to their ability to effectively inhibit bacterial and fungal growth.<sup>5</sup>

In healthcare settings, long-surviving pathogens can be transmitted through patients, healthcare personnel, and equipment, leading to hospital-acquired infections (HAIs). Highly contagious epidemic viruses, such as influenza, SARS-CoV, and SARS-CoV-2, can also cause hospital infections and community transmission. Thus, reducing the spread of viruses within healthcare facilities has become a critical focus of modern infection prevention strategies. In this case, antimicrobial agents are commonly applied to hospital textiles to mitigate infections. For example, treating hospital bed linens with antimicrobial agents can reduce bacterial colonization and curb the growth of pathogens such as methicillin-resistant *Staphylococcus aureus* (MRSA) and vancomycin-resistant *Enterococcus* (VRE), thereby decreasing HAIs.<sup>6–8</sup> However, textiles require post-treatment with antimicrobial agents after each wash, making this method inconvenient and costly. As a result, extensive research has been conducted to develop

<sup>a</sup> Department of Applied Science, National Taitung University, 369, Sec. 2, University Rd., Taitung City 95092, Taiwan. E-mail: ccwu@nttu.edu.tw; Fax: +886-89-318855

<sup>b</sup> DAZZEON Technology, 4F, No. 81, Sec. 4, Chengde Rd., Shilin District, Taipei City 11166, Taiwan. Fax: +886-2-23258737

† Electronic supplementary information (ESI) available: Thermogravimetric analysis, digital and SEM images, zeta potential measurement results, and antimicrobial activity. See DOI: <https://doi.org/10.1039/d4ma00650j>



antimicrobial textiles with durable properties. The use of antibacterial textiles can minimize microbial colonization, reducing the risk of infections from fabrics such as sheets, towels, and gowns. Incorporating copper oxide and copper composites into biocidal textiles for use in long-term care settings has been shown to significantly reduce HAIs, fever occurrences, antibiotic use, and medical resource consumption.<sup>8–10</sup>

Key antimicrobial textile technologies include noble metal nanoparticle technology,<sup>11</sup> bio-based antimicrobial agents,<sup>12</sup> photocatalytic technology,<sup>13</sup> antimicrobial coating technology,<sup>14</sup> and smart antimicrobial textiles.<sup>15</sup> Among them, noble metal nanoparticles have emerged as a highly effective and widely studied approach. Noble metals exert strong antimicrobial activity by disrupting microbial cell membranes, inhibiting enzymatic functions, and interfering with DNA replication, thereby exhibiting bactericidal effects.<sup>16</sup>

In noble metal nanoparticle technology, metals such as gold (Au), silver (Ag), and copper (Cu) are used to develop antimicrobial textiles.<sup>17–24</sup> However, although silver nanoparticles have been extensively studied for their biocidal properties, few studies have explored the antimicrobial potential of Au and Cu. Gold nanoparticles have also attracted attention due to their unique physical and chemical properties. In this case, although Ag nanoparticles are more commonly used and typically exhibit stronger antimicrobial effects, gold nanoparticles possess notable antimicrobial activity. Additionally, Au nanoparticles have excellent biocompatibility and non-toxicity, making them suitable for antimicrobial textile applications.<sup>17</sup> Copper, an essential trace element naturally present in plant and animal tissues, plays a crucial role in human metabolism. Moreover, Cu is significantly cheaper than Au and Ag, making it a cost-effective alternative for developing antimicrobial and antiviral textiles.

Recent studies have shown that different forms of Cu (*e.g.*, Cu(0), copper oxide, ionic copper, and copper-polymer composites) exhibit antimicrobial and antiviral properties, particularly at the nanoscale.<sup>24</sup> However, the underlying mechanisms for the antimicrobial and antiviral activity of Cu are not yet fully understood. It has been proposed that they involve the release of copper ions ( $\text{Cu}^{2+}$ ), cell membrane damage, reactive oxygen species (ROS) generation, and bacterial metabolic disruption. A study demonstrated that coronaviruses survive on Cu surfaces for less than four hours, whereas they persist on plastic surfaces for over 72 hours.<sup>25</sup> Furthermore, Behzadinasab *et al.* reported that  $\text{Cu}_2\text{O}$ /PU composite coatings significantly reduced the infectious titer of SARS-CoV-2, achieving a 99.9% reduction within one hour compared to the uncoated samples.<sup>26</sup> Consequently, Cu has regained attention due to its excellent antimicrobial characteristics. A review of clinical and animal studies confirmed that textiles containing copper oxide had no adverse effects on human skin.<sup>27</sup> Additionally, a 2009 report by the Environmental Protection Agency found no systemic toxicity or occupational risks associated with Cu exposure. The release of copper ions ( $\text{Cu}^{2+}$ ) results in cell membrane damage catalyzed by reactive oxygen species (ROS), bacterial DNA degradation, metal-thiol interactions, and synergistic effects.<sup>28–40</sup>

The functionalization of textiles with noble metals requires that their antimicrobial performance remains stable throughout their use, making it necessary to firmly embed them onto textiles. Various methods exist for incorporating noble metal nanoparticles into textiles, including surface coating (*e.g.*, dip-coating and spray-coating), *in situ* synthesis, and electrospinning. However, traditional coating techniques, such as spraying, result in  $\text{Cu}_2\text{O}$  nanoparticles being physically adsorbed onto textiles *via* van der Waals forces, leading to reduced antimicrobial effectiveness after washing. Similar results were observed when cotton fabrics were padded in salt noble metal solutions.<sup>41</sup> A. Errokh *et al.* demonstrated that chemically immobilized  $\text{Cu}_2\text{O}$  nanoparticles could serve as sacrificial templates to anchor noble metals onto textiles.<sup>42</sup> In the study by the Emama group, oxidizing agents such as hydrogen peroxide ( $\text{H}_2\text{O}_2$ ) and sodium hydroxide (NaOH) were used to increase the content of carboxyl groups on cotton fabric surfaces. Although some CuO and  $\text{TiO}_2$  were lost after multiple wash cycles, the antibacterial effect remained significant.<sup>43,44</sup> Other techniques, such as grafting polymer brushes onto fabrics, enhanced the durability and maintained the long-term antibacterial efficacy of the fabrics.<sup>45,46</sup> Additionally, cross-linkers improved the adhesion between noble metals and fabrics; however, their complex manufacturing processes limit their commercial feasibility.<sup>47,48</sup> Researchers have also developed multifunctional antimicrobial textiles with properties such as dyeability, UV protection, water repellency, and photoluminescence, adding significant commercial value.<sup>49–56</sup>

For noble metal-based antimicrobial textiles to achieve commercial viability, their antimicrobial efficacy must remain stable over repeated use. Unlike previous techniques that incorporate antimicrobial agents after fabric processing, this study focuses on embedding  $\text{Cu}_2\text{O}$  nanoparticles into masterbatches, specifically in their lower oxidation state. To the best of our knowledge, no previous research has explored the impregnation of Cu or its derivatives into masterbatches, followed by spinning and weaving them into textiles. We fabricated two types of masterbatches,  $\text{Cu}_2\text{O}$  NPs embedded in polypropylene (PP) and polyethylene terephthalate (PET). This approach prevented  $\text{Cu}_2\text{O}$  from detaching from the textile surface and inhibited its oxidation into CuO. Studies have shown that  $\text{Cu}_2\text{O}$  exhibits higher antimicrobial activity than CuO due to the greater release of  $\text{Cu}^+$  ions.<sup>57–59</sup> However,  $\text{Cu}_2\text{O}$  is prone to oxidation, which reduces its antimicrobial efficiency.

To validate our approach, we used  $\text{Cu}_2\text{O}$  NP-embedded PP masterbatches to produce melt-blown nonwoven fabric products. Our method aligns with conventional textile industry manufacturing techniques. The  $\text{Cu}_2\text{O}$  NP-PET melt-blown nonwoven fabrics fabricated using this technique exhibited excellent antimicrobial activity against both Gram-negative and Gram-positive bacteria, even after being stored for an extended period or undergoing 50 washing cycles. This durability is attributed to the antioxidant property of  $\text{Cu}_2\text{O}$  and its strong adhesion to PP. The high stability of  $\text{Cu}_2\text{O}$  NP-embedded PP for



antimicrobial melt-blown nonwoven fabrics has not been reported in previous Cu<sub>2</sub>O-based research.

## Experimental section

### Materials and Cu<sub>2</sub>O solution

Cu<sub>2</sub>O powder was purchased from Taixing Smelting Plant (Cu<sub>2</sub>O ≥ 98%, average diameter = 25 μm). Before use, the powder was dried at 150 °C overnight to remove absorbed moisture. The Cu<sub>2</sub>O solution was prepared by dispersing 20% (by mass) of Cu<sub>2</sub>O in water, using poly(propylene glycol) (purchased from EVONIK) as the dispersant. Polypropylene (PP) and polyethylene terephthalate (PET) powders, used as fiber raw materials, were obtained from Yuang Shen and David & Mike in Taiwan, respectively.

### Synthesis of Cu<sub>2</sub>O masterbatches

To ensure homogeneous mixing of the Cu<sub>2</sub>O nanoparticles (NPs) with PP or PET powder, the Cu<sub>2</sub>O solution was wet-milled using a NETZSCH LMZ10 system. This process refined the particles from 25 μm to the submicron scale. Subsequently, the refined Cu<sub>2</sub>O powder was spray-dried at 150 °C. Next, a mixture of 12 wt% refined Cu<sub>2</sub>O powder and 88 wt% PP or PET fiber raw material was prepared for masterbatch production. The mixture underwent compression, melting, extrusion, and pelletization using an extrusion-pelletizing machine from Kowin Recycling Machine, yielding Cu<sub>2</sub>O NP-embedded masterbatches (Cu<sub>2</sub>O NP-embedded PP or Cu<sub>2</sub>O NP-embedded PET).

### DLS and zeta potential measurements

The particle size distribution of the fine powders and the zeta potential of the Cu<sub>2</sub>O NP-embedded PP masterbatches and nonwoven fabrics were analyzed using a Particulate Systems Nano Plus HD zeta/nanoparticle analyzer. In the dynamic light scattering (DLS) measurements, a 660-nm laser was directed at the prepared aqueous solution, and backscattered signals were collected using an avalanche photodiode detector at an angle of 165°. For the zeta potential measurements, the fabric samples were cut into 15 mm (*W*) × 35 mm (*L*) pieces. These samples were placed on a quartz crystal with an open side in the solid sample cell, where their zeta potential was measured. Subsequently, the quartz crystal was filled with reference polystyrene (PS) latex particles provided by Particulate Systems. A voltage was applied to the platinum electrodes, and the electroosmotic flow in the solid sample cell generated asymmetrical parabolic velocity profiles due to the charge differences on the upper and lower surfaces. These differences were analyzed using the Mori and Okamoto equation.<sup>60</sup> The apparent electrophoretic mobility at different cell positions was measured and converted into zeta potential using the Smoluchowski equation.<sup>61</sup>

### Characterization

SEM images of the masterbatches and powder suspension were obtained using a Hitachi S-4800. The morphologies of Cu<sub>2</sub>O

NP-PP and Cu<sub>2</sub>O NP-PET meltblown nonwoven fabrics were characterized using a Thermo Scientific Phenom XL G2, which collects backscattered electrons and is equipped with an EDS system for elemental analysis. A TA instrument Q500 was used to perform TGA in a nitrogen atmosphere in the temperature range of 30 °C to 900 °C (heating rate: 10 °C min<sup>-1</sup>). The crystallinity of the samples was examined using a Bruker D8 Discover diffractometer. XPS was performed using a Thermo Scientific K-Alpha X-ray photoelectron spectrometer with an Al Kα micro-focused monochromator as the radiation source. Before the measurement, a 6-nm surface of the PP masterbatch was sputtered with Ar ions to expose the embedded ingredients. The location of any color of textiles in the space was determined by its color coordinates; *L*\*, *a*\*, and *b*\*. The object was measured using the Datacolor<sup>®</sup> 500 family of benchtop spectrophotometers.

### Evaluation of antimicrobial activity

The antimicrobial activity of the Cu<sub>2</sub>O NP-embedded melt-blown nonwoven fabrics was assessed according to JIS L 1902:2015. The bacterial viability was evaluated using the pour plate method. The test organisms included Gram-negative bacteria (*Pseudomonas aeruginosa* ATCC 10145, *Escherichia coli* ATCC 8739, and *Klebsiella pneumoniae* ATCC 4352), Gram-positive bacteria (*Staphylococcus aureus* ATCC 6538P and methicillin-resistant *Staphylococcus aureus* (MRSA) ATCC 33591), and fungi (*Candida albicans* ATCC 10231). Briefly, 1 mL of bacterial culture grown in nutrient broth was spread onto an agar plate. The Cu<sub>2</sub>O NP-embedded meltblown nonwoven fabrics were placed over the plates, while the control plates were left uncovered. The plates were incubated at 37 °C ± 1 °C for 18–24 h. The bacterial count (colony-forming units per milliliter, CFU per mL) was determined before and after incubation.

### Laundrying

The antimicrobial activity of the Cu<sub>2</sub>O NP-embedded melt-blown nonwoven fabrics after washing was evaluated following AATCC 135-2018, a standard established by the American Association of Textile Chemists and Colorists (AATCC). The fabrics were washed at 30 °C ± 3 °C and dried at temperatures below 60 °C for 50 cycles. After laundrying, antimicrobial activity tests were conducted to assess the retention of antibacterial properties.

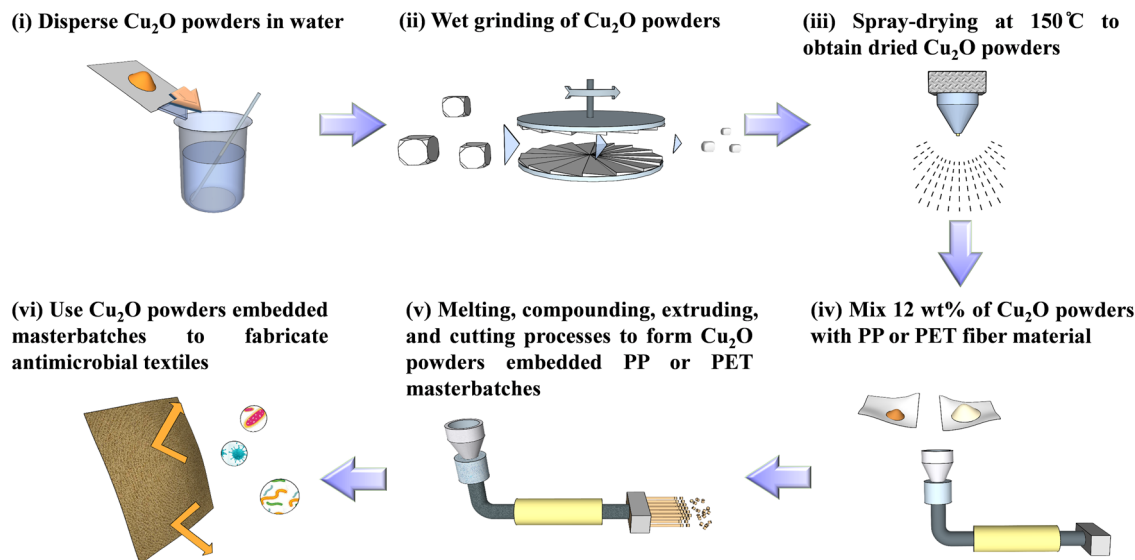
## Results and discussion

### Synthesis of Cu<sub>2</sub>O NP-embedded masterbatches and Cu<sub>2</sub>O-embedded textiles

Scheme 1 illustrates the process for the preparation of Cu<sub>2</sub>O NP-embedded masterbatches. Briefly, Cu<sub>2</sub>O NP-embedded masterbatches were synthesized using a 20 wt% aqueous solution of Cu<sub>2</sub>O NPs. The particles were wet-milled to obtain a fine powder suspension. The dynamic light scattering (DLS) analysis revealed that the hydrodynamic diameter of the fine powder







Scheme 1 Schematic of the preparation of  $\text{Cu}_2\text{O}$  NP-embedded masterbatches.

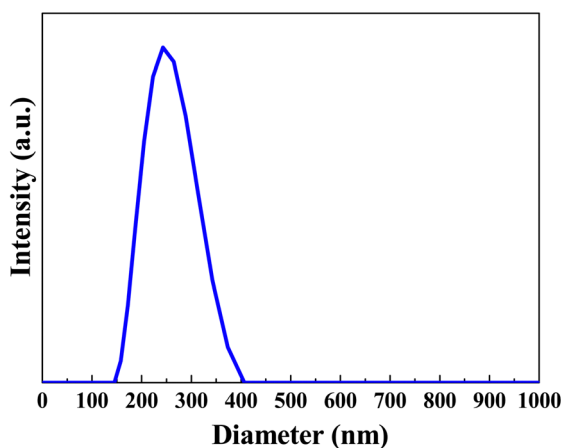


Fig. 1 Hydrodynamic diameter of  $\text{Cu}_2\text{O}$  NPs powders after the grinding process.

was 306 nm (Fig. 1). Subsequently, the suspension was spray-dried to yield dried powders, which were mixed with either PP or PET. Next, a continuous process involving compression, melting, extrusion, and cutting was employed to produce  $\text{Cu}_2\text{O}$  NP-embedded masterbatches (Fig. 2(a)). To fabricate yarns and textiles, 12 wt%  $\text{Cu}_2\text{O}$  NP-embedded (PP or PET) masterbatches were homogeneously blended with raw PP or PET masterbatches through melting and fusion processes. The thermogravimetric analysis (TGA) results for the  $\text{Cu}_2\text{O}$  NP-embedded PP masterbatches are presented in Fig. S1 (ESI<sup>†</sup>), demonstrating that the final degradation temperature and residual  $\text{Cu}_2\text{O}$  concentration were 467.7 °C and 11.33%, respectively. Fig. 2(b) shows a roll of the meltblown nonwoven fabric produced using the  $\text{Cu}_2\text{O}$  NP-embedded PP masterbatches (hereafter referred to as  $\text{Cu}_2\text{O}$  NP-PP meltblown nonwoven fabric), which can be utilized for fabricating face masks as one potential application (Fig. S2a, ESI<sup>†</sup>). Additionally, this

approach can be extended to produce various fiber-based materials and different types of  $\text{Cu}_2\text{O}$  NP-embedded textiles with antimicrobial properties. Fig. S2b and c (ESI<sup>†</sup>) illustrate the  $\text{Cu}_2\text{O}$  NP-embedded PET masterbatches and  $\text{Cu}_2\text{O}$  NP-embedded PET meltblown nonwoven fabric (hereafter referred to as  $\text{Cu}_2\text{O}$  NP-PET meltblown nonwoven fabric), respectively.

### Morphology and crystallinity

Fig. 3(a), (b), and (d) present the scanning electron microscopy (SEM) images of the  $\text{Cu}_2\text{O}$  solution containing fine powders after grinding,  $\text{Cu}_2\text{O}$  NP-embedded PP masterbatches, and meltblown nonwoven fabric produced using  $\text{Cu}_2\text{O}$  NP-embedded PP masterbatches, respectively. As shown in Fig. 3(a), the average particle size of  $\text{Cu}_2\text{O}$  NPs after grinding was 306 nm. Fig. 3(b) shows the SEM image of the  $\text{Cu}_2\text{O}$  NP-embedded PP masterbatch, where the black regions correspond to PP, while the white and gray particles represent  $\text{Cu}_2\text{O}$  NPs. The  $\text{Cu}_2\text{O}$  NPs were observed to be uniformly distributed within the PP masterbatches. The chemical composition of the  $\text{Cu}_2\text{O}$  NP-embedded PP masterbatches was analyzed using energy-dispersive X-ray spectroscopy (EDS). Fig. 3(c) confirms the presence of Cu in the  $\text{Cu}_2\text{O}$  NP-embedded PP masterbatches. Fig. 3(d) illustrates the meltblown nonwoven fabric fabricated using the  $\text{Cu}_2\text{O}$  NP-embedded PP masterbatches. Additionally, Fig. S3 (ESI<sup>†</sup>) presents the elemental mapping of the meltblown nonwoven fabric produced from the  $\text{Cu}_2\text{O}$  NP-embedded PP masterbatches. As depicted in Fig. S3 (ESI<sup>†</sup>), carbon (C) exhibited the highest concentration in the meltblown nonwoven fabric, followed by oxygen (O), whereas the concentration of Cu was relatively low. This is because only 12 wt% of  $\text{Cu}_2\text{O}$  NPs was incorporated into the meltblown nonwoven fabric produced from the  $\text{Cu}_2\text{O}$  NP-embedded PP masterbatches. Fig. S4 (ESI<sup>†</sup>) further displays the meltblown nonwoven fabric fabricated using the  $\text{Cu}_2\text{O}$  NP-embedded PET masterbatches.



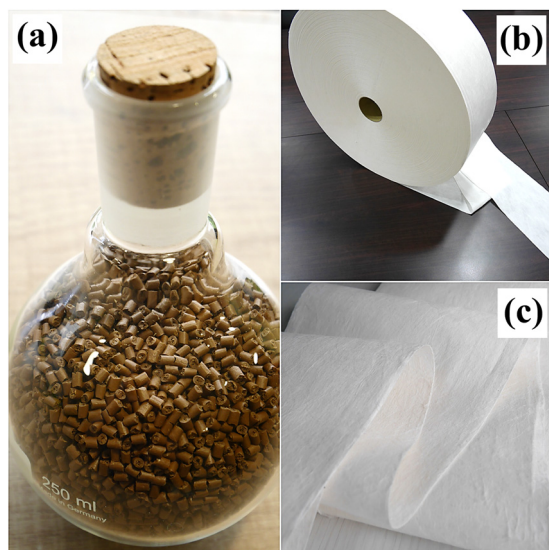


Fig. 2 Digital images of (a)  $\text{Cu}_2\text{O}$  NP-embedded PP masterbatches and (b) a roll of  $\text{Cu}_2\text{O}$ -PP meltblown nonwoven fabric. This fabric was used for the evaluation of antimicrobial activity in the present study. (c) Closer view of (b).

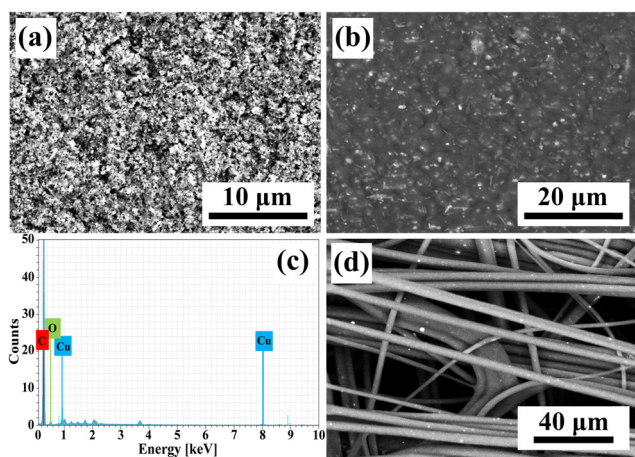


Fig. 3 SEM images of (a) fine powder suspension and (b) the  $\text{Cu}_2\text{O}$  NP-embedded PP masterbatch. (c) EDS spectrum of  $\text{Cu}_2\text{O}$  NP-PP meltblown nonwoven fabrics made from the  $\text{Cu}_2\text{O}$  NP-embedded PP masterbatch. (d)  $\text{Cu}_2\text{O}$  NP-PP meltblown nonwoven fabrics.

Fig. 4 shows the X-ray diffraction (XRD) patterns of the  $\text{Cu}_2\text{O}$  nanoparticles (NP) and  $\text{Cu}_2\text{O}$  NP-embedded polypropylene (PP) masterbatches. The diffraction peaks of  $\text{Cu}_2\text{O}$  NP at  $2\theta$  values of  $36.5^\circ$ ,  $42.7^\circ$ ,  $47.1^\circ$ ,  $61^\circ$ , and  $76.7^\circ$  were assigned to the (111), (200), (211), (200), and (111) planes of  $\text{Cu}_2\text{O}$ , respectively (JCPDS no. 05-0667). No  $\text{CuO}$  phase, secondary phases, or unknown phases were observed, as shown in Fig. 4(a). Fig. 4(b) presents the XRD pattern of the  $\text{Cu}_2\text{O}$  NP-embedded PP masterbatches. The (131), (301), (060), and (220) planes of PP were observed at  $2\theta$  values of  $21.1^\circ$ ,  $21.8^\circ$ ,  $25.4^\circ$ , and  $28.6^\circ$ , respectively.<sup>62</sup> The same diffraction peaks of  $\text{Cu}_2\text{O}$  NP at  $2\theta$  values of  $36.5^\circ$ ,  $42.7^\circ$ ,  $47.1^\circ$ ,  $61^\circ$ , and  $76.7^\circ$  were assigned to the

(111), (200), (211), (200), and (111) planes, respectively. The very weak peaks at  $36.1^\circ$  and  $38.9^\circ$  were attributed to the (002) and (111) planes of  $\text{CuO}$ , respectively (JCPDS no. 48-1548). The XRD results suggest that slight oxidation of  $\text{Cu}_2\text{O}$  occurred during the fabrication of the masterbatches; however, this did not affect the antimicrobial properties of the textiles.

### Chemical bonding state

The chemical composition of the  $\text{Cu}_2\text{O}$  NP-embedded polypropylene (PP) masterbatches was examined using X-ray photoelectron spectroscopy (XPS), as shown in Fig. 5. The survey spectrum in Fig. 5(a) revealed the presence of carbon (C), oxygen (O), and copper (Cu) elements, with the corresponding photoelectron peaks located at binding energies of 287 eV (C 1s), 531 eV (O 1s), 933.6 eV (Cu 2p), 76 eV (Cu 3p), and 122 eV (Cu 3s).

Fig. 5(b) shows the high-resolution scan of the Cu 2p core-level spectrum. The characteristic doublet peaks centered at 933.6 and 953.7 eV correspond to Cu  $2p_{3/2}$  and Cu  $2p_{1/2}$ , respectively. Deconvolution of the Cu 2p electron binding energy revealed five peaks after Gaussian fitting at 932.7, 934.5, 947.6, 952.8, and 954.6 eV. The peaks at 932.7 and 952.8 eV were attributed to the Cu  $2p_{3/2}$  and Cu  $2p_{1/2}$  peaks of  $\text{Cu}^+$  ions, confirming the presence of  $\text{Cu}_2\text{O}$ .<sup>63</sup> The weak peaks at 934.5 and 954.6 eV were assigned to the Cu  $2p_{3/2}$  and Cu  $2p_{1/2}$  peaks of  $\text{Cu}^{2+}$  ions, indicating the presence of  $\text{CuO}$ .<sup>64,65</sup> The peak intensities for  $\text{Cu}_2\text{O}$  (932.7 and 952.8 eV) were higher than that for  $\text{CuO}$  (934.5 and 954.6 eV). Additionally, weak shake-up satellite bands were observed at 942–950 eV (with a peak at 947.6 eV), further suggesting the formation of  $\text{Cu}^{2+}$  ions.<sup>66–68</sup> Shake-up bands occur when scattering photoelectrons interact with a valence electron, exciting it to a higher energy level. As a result, the kinetic energy of the core electron is slightly reduced, producing a satellite structure a few eV below the core-level position. The XPS results indicate that the  $\text{Cu}^+$  ions have a filled electron configuration of  $[\text{Ar}]3d^{10}$ , while the  $\text{Cu}^{2+}$  ions have an unfilled  $[\text{Ar}]3d^9$  configuration, with unpaired electrons in their d orbital. The photoelectrons collide with these d-electrons, exciting them to a higher energy level and reducing the kinetic energy of the 2p valence electrons. This interaction leads to the appearance of both a major XPS peak for  $\text{Cu}^{2+}$  ions and satellite peaks due to the interaction of the Cu 2p electron emission with the secondary excitation of outer valence electrons.<sup>69</sup> These XPS results demonstrate that Cu ions in the  $\text{Cu}_2\text{O}$  NP-embedded PP masterbatches exist in both the  $\text{Cu}^+$  and  $\text{Cu}^{2+}$  chemical states. This  $\text{Cu}^+$  and  $\text{Cu}^{2+}$  composition is likely due to the manufacturing process, which involves melting the PP fiber raw material at temperatures of around  $250\text{--}260^\circ\text{C}$ , leading to the slight oxidation of  $\text{Cu}_2\text{O}$  NPs.

To assess the stability of the  $\text{Cu}_2\text{O}$  NP-embedded PP masterbatch in air, it was exposed to air for 12 months, and subsequently examined using XPS (Fig. S5, ESI†). The peak intensity of  $\text{Cu}^+/\text{Cu}^{2+}$  at 933.6 eV for the  $\text{Cu}_2\text{O}$  NP-embedded masterbatch exposed to air for 6 months was 1.17, which is similar to the peak intensity observed for the as-fabricated masterbatch that was not exposed to air. This result suggests





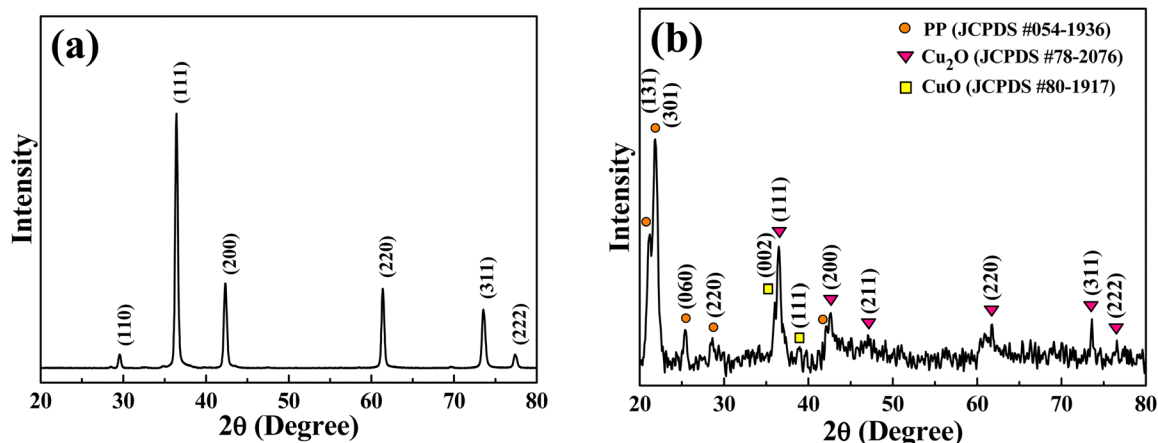


Fig. 4 X-ray diffraction patterns of (a)  $\text{Cu}_2\text{O}$  NP and (b)  $\text{Cu}_2\text{O}$  NP-embedded PP masterbatches.

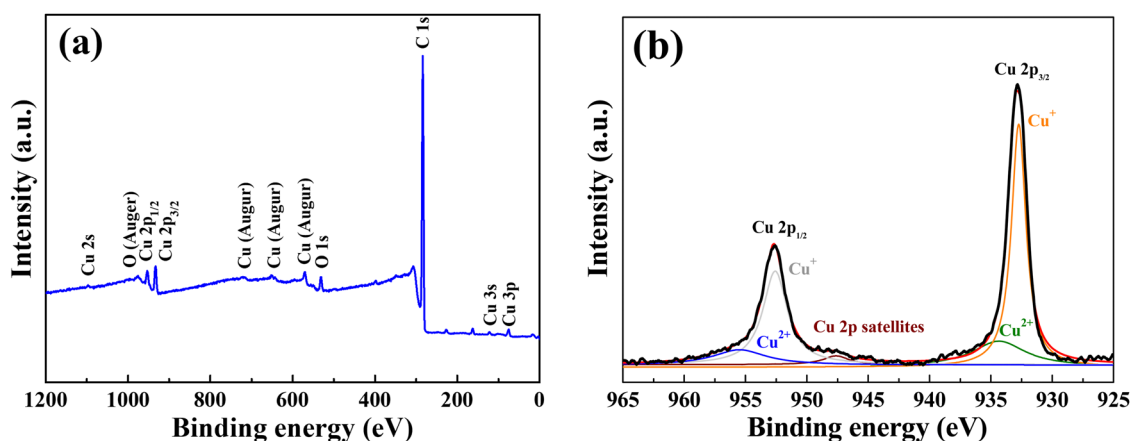


Fig. 5 XPS characterization of  $\text{Cu}_2\text{O}$  NP-embedded PP masterbatch. (a) Survey scan and (b) high-resolution Cu 2p spectra.

that the  $\text{Cu}_2\text{O}$  NPs in the PP polymer matrix were not further oxidized during the 6-month exposure to air. This stability can be attributed to the PP polymer, which isolates the  $\text{Cu}_2\text{O}$  NPs from moisture and oxygen in the air, preventing their further oxidation.

### Color coordinates

To understand the effect of the incorporation of  $\text{Cu}_2\text{O}$  NPs on the dyeing performance of antimicrobial textiles, the samples were evaluated using the CIE  $L^*a^*b^*$  (CIELAB) color space coordinates. The brightness value ( $L^*$ ) of the pure PP textile was 94.31, with  $a^*$  and  $b^*$  values of 0.47 and 3.38, respectively. In the case of the  $\text{Cu}_2\text{O}$  NP-embedded PP textiles, their color coordinates were  $L^* = 66.12$ ,  $a^* = 1.92$ , and  $b^* = 18.2$ , as shown in Table S1 (ESI<sup>†</sup>). Additionally, the  $K/S$  value of the pure PP textile was 0.143, while the value for the  $\text{Cu}_2\text{O}$  NP-embedded PP textile was 0.191.

### Antimicrobial activity

The electrostatic interaction between positively charged metal ions and the negatively charged cell walls of bacteria can trigger

antimicrobial activity. It has been shown that the surface charge of silver (Ag) NPs significantly affects their antimicrobial properties. Positively charged Ag NPs exhibit a stronger antimicrobial effect than neutral or negatively charged Ag NPs. Thus, to investigate the surface charge of the fabrics prepared with Cu-embedded PP masterbatches, we measured the surface zeta potential of the meltblown nonwoven fabrics made with  $\text{Cu}_2\text{O}$  NP-embedded PP (Fig. S6, ESI<sup>†</sup>). The results revealed that the surface zeta potential of the meltblown nonwoven fabric was close to zero, indicating that it had a neutral surface, which resulted from the electrostatic treatment during the final spinning process.

To evaluate the antimicrobial activity of the meltblown nonwoven fabrics made with the  $\text{Cu}_2\text{O}$  NP-embedded PP masterbatches, tests were conducted according to the Japanese Industrial Standard (JIS) L 1902:2015. Five bacterial species were used to assess their antimicrobial activity, as shown in Fig. 6, including Gram-positive bacteria (*S. aureus* and MRSA), Gram-negative bacteria (*Escherichia coli*, *Pseudomonas aeruginosa*, and *Klebsiella pneumoniae*), and the fungus *Candida albicans*. The left column of Fig. 6 shows the bacterial count



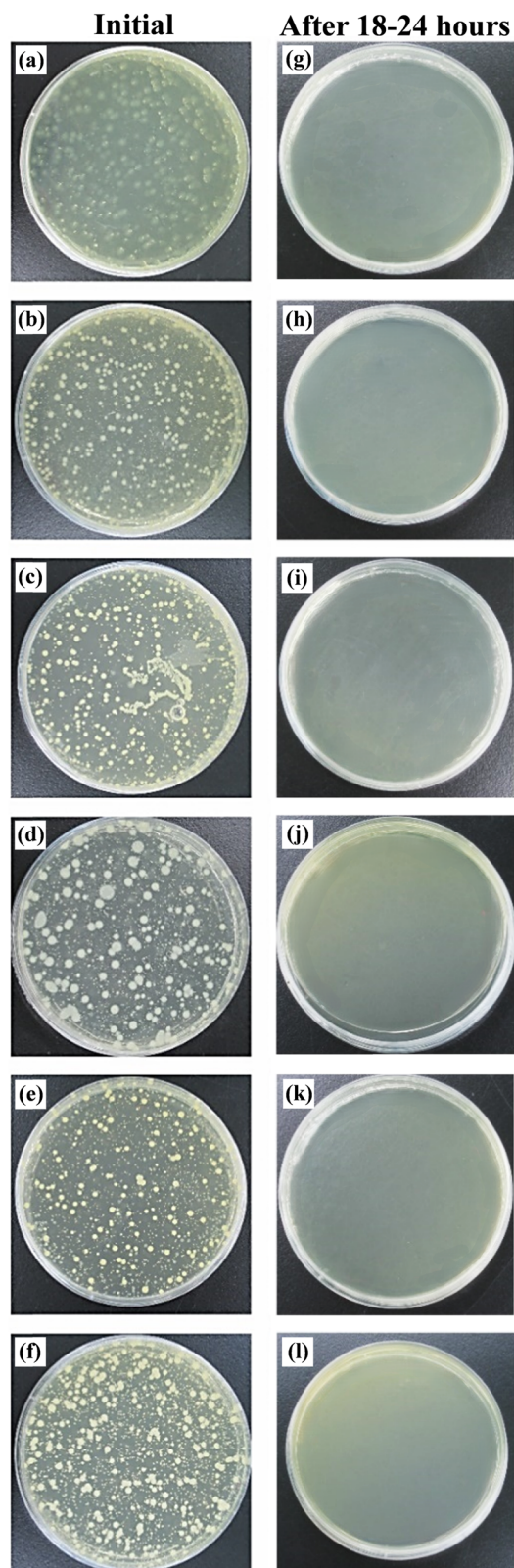


**Fig. 6** Antimicrobial activity of  $\text{Cu}_2\text{O}$  NP-PP meltblown nonwoven fabrics against different species of microorganisms. The left column presents the pictures of the test just begun, and the right column depicts the results after 18–24 h. (a) and (g) *P. aeruginosa*. (b) and (h) *E. coli*. (c) and (i) Methicillin-resistant *Staphylococcus aureus* (MRSA). (d) and (j) *S. aureus*. (e) and (k) *K. pneumoniae*. (f) and (l) *C. albicans*.

(approximately  $3 \times 10^4$  CFU per mL) immediately after inoculating the samples with the bacterial inoculum, while the right column shows the bacterial count after 18–24 h of incubation. Fewer than 20 colony-forming units per milliliter (CFU per mL) of Gram-positive bacteria, Gram-negative bacteria, and fungi were observed on the agar plates. The antibacterial activity (A) of the fabrics was calculated using the formula defined by the Japan Textile Evaluation Technology Council to evaluate the antimicrobial properties of textiles, as follows:

$$A = (\log C_t - \log C_0) - (\log T_t - \log T_0),$$

if  $\log C_0 > \log T_0$ , then  $A = C_t - T_t$

where  $C_0$  is the bacterial count observed immediately after inoculation on the standard fabric,  $C_t$  is the bacterial count observed after 18–24 h of incubation on the standard fabric,  $T_0$  is the bacterial count noted immediately after inoculation on the fabrics made with  $\text{Cu}_2\text{O}$  NP-embedded PP masterbatches, and  $T_t$  is the bacterial count observed after 18–24 h of incubation on the fabrics made with  $\text{Cu}_2\text{O}$  NP-embedded PP masterbatches. A value greater than 3 indicates that the textile is highly effective against microorganisms. Fig. 7 shows a comparison of the antimicrobial activity of the standard fabric (control) with the meltblown nonwoven fabrics made with the  $\text{Cu}_2\text{O}$  NP-embedded PP masterbatches. The left column shows the results immediately after inoculation of the test bacteria, and the right column shows the results after 18–24 h of

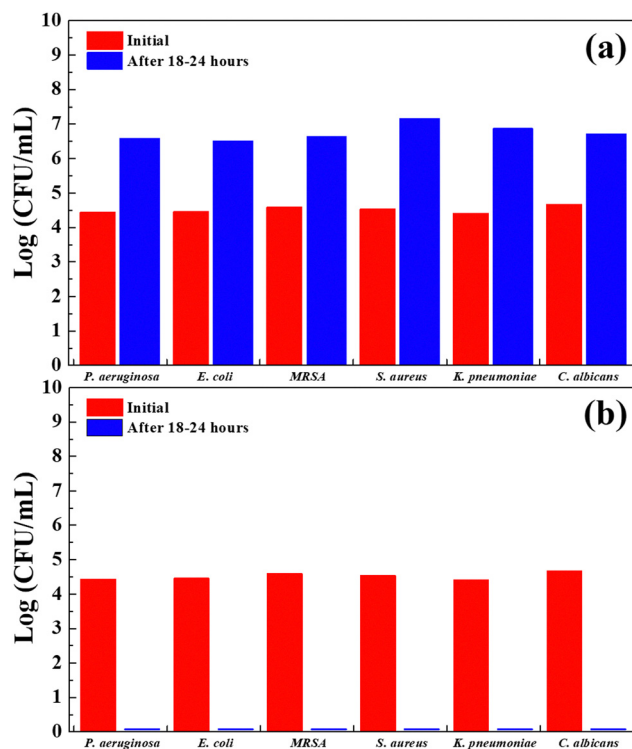


**Fig. 7** Histograms representing the antimicrobial activity of  $\text{Cu}_2\text{O}$  NP-PP meltblown nonwoven fabrics against microorganisms. (a) Tests using the control. No  $\text{Cu}_2\text{O}$  NP-PP meltblown nonwoven fabric was placed in the agar plates in these tests. (b) Tests with the presence of  $\text{Cu}_2\text{O}$  NP-PP meltblown nonwoven fabrics.



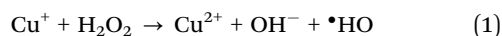


incubation. The results indicate that the meltblown nonwoven fabrics made with Cu<sub>2</sub>O NP-embedded PP effectively inhibited bacterial growth.

The antimicrobial properties of Cu<sub>2</sub>O NPs primarily rely on the release of Cu<sup>+</sup> ions, which damage the cellular structure of microorganisms and disrupt their physiological functions. The antibacterial mechanism of Cu<sub>2</sub>O NPs involves the release of free Cu ions, which catalyze the formation of reactive oxygen species (ROS) such as superoxide anions (O<sub>2</sub><sup>•−</sup>), hydrogen peroxide (H<sub>2</sub>O<sub>2</sub>), hydroxyl radicals (•OH), and organic hydroperoxides in a Fenton-like reaction. These ROS damage cellular components and penetrate bacterial cells, leading to microbial cell death.<sup>29–32</sup>

Given that Gram-positive bacteria (*S. aureus* and MRSA) lack a thick outer membrane that acts as a barrier to reactive oxygen species (ROS), the hydroxyl radicals (•OH) generated by Cu ions cause structural changes in phospholipids and disrupt the membrane integrity. Cu<sup>+</sup> ions can pass through the cell membrane, leading to DNA degradation.

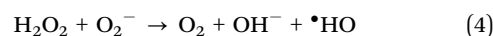
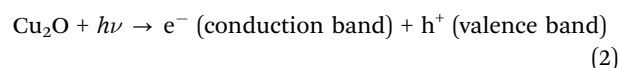
Fig. 8 presents a proposed model illustrating the antibacterial mechanisms of the meltblown nonwoven fabrics prepared using Cu<sub>2</sub>O NP-embedded PP masterbatches when exposed to Gram-positive bacteria. Firstly, the Fenton reaction (eqn (1)) occurs, where Cu<sup>+</sup> ions react with hydrogen peroxide (H<sub>2</sub>O<sub>2</sub>) to produce hydroxyl radicals, which degrade the peptidoglycan layer of the bacterial cell. In this process, Cu<sup>+</sup> ions are released from the Cu<sub>2</sub>O NP-embedded PP masterbatch.



Next, Cu<sup>+</sup> ions enter the periplasmic space, separating the cytosol from the plasma membrane, which leads to membrane damage. This process follows one of the following pathways: (A) → (B), (A) → (B) → (C) → (b), or (A) → (B) → (C) → (c).

Following this, Cu<sup>+</sup> ions penetrate the cell membrane, catalyzing ROS formation, which ultimately leads to DNA degradation. This pathway follows one of the following mechanisms: (a) → (b) or (a) → (c).

An additional minor antibacterial mechanism of Cu<sub>2</sub>O NPs involves a photocatalytic reaction. Cu<sub>2</sub>O has a direct bandgap of 2.1 eV. When visible light ( $\lambda > 410$  nm) strikes the surface of Cu<sub>2</sub>O NPs, an electron can jump from the valence band to the conduction band, as shown in eqn (2). Subsequently, the generated electrons are scavenged by molecular oxygen to form superoxide anions (O<sub>2</sub><sup>•−</sup>), as shown in eqn (3). O<sub>2</sub><sup>•−</sup> reacts with H<sub>2</sub>O<sub>2</sub> to produce hydroxyl radicals (•HO), as shown in eqn (4). These hydroxyl radicals are the key oxidizing agents that damage bacterial cells.



Furthermore, the electrons generated in this reaction are paired, creating free radicals. These free radicals scavenge other electrons within the bacterial cells, pairing with them and causing damage to the cell wall, DNA, and proteins.

The mechanism by which Cu inhibits the growth of *E. coli* involves hydroxyl radicals induced by Cu ions, which drive the nonenzymatic peroxidation of unsaturated fatty acids in the bacterial cell membrane. This reaction initiates a chain process that leads to structural changes in phospholipids and disrupts the membrane integrity.<sup>69</sup> A similar mechanism is involved in the Cu-mediated inhibition of *P. aeruginosa* and *K. pneumoniae* growth. Fig. 9 illustrates how the Cu<sub>2</sub>O NP-PP meltblown nonwoven fabrics inhibit the growth of Gram-negative bacteria.

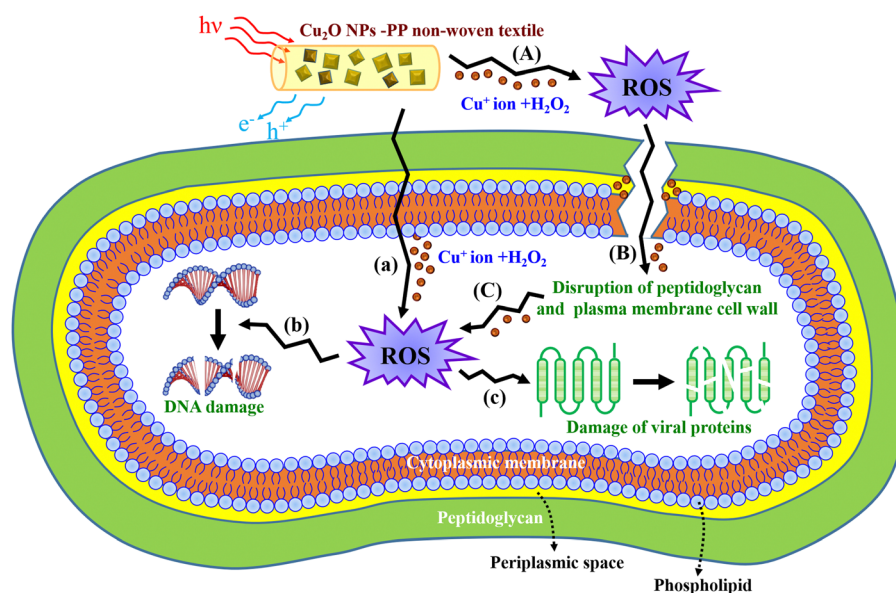


Fig. 8 Schematic of the probable antimicrobial mechanism of Cu<sub>2</sub>O NP-PP meltblown nonwoven fabrics against Gram-positive bacteria.



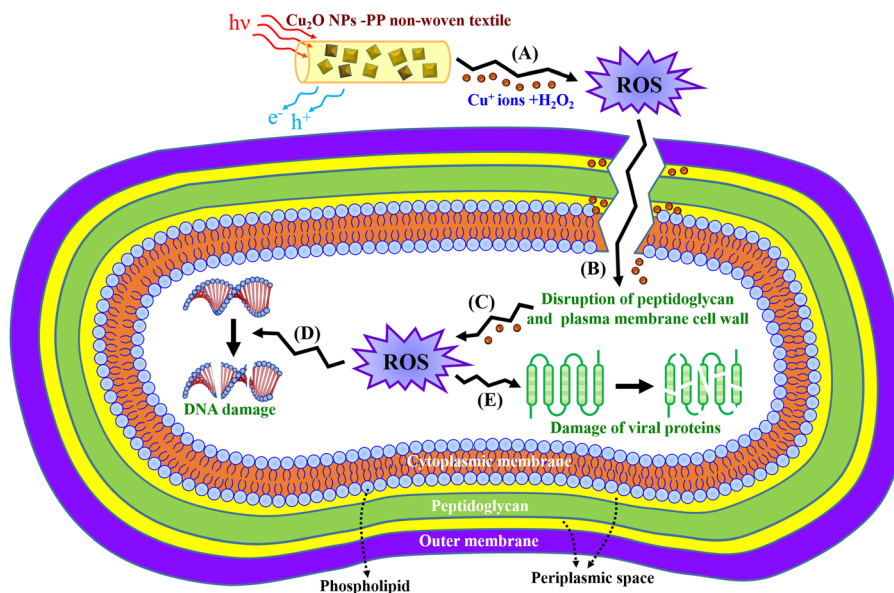


Fig. 9 Schematic of the probable antimicrobial mechanism of  $\text{Cu}_2\text{O}$  NP-PP meltblown nonwoven fabrics against Gram-negative bacteria.

Gram-negative bacteria have a three-layered cell envelope, consisting of an outer membrane, peptidoglycan, plasma membrane, and periplasmic space.  $\text{Cu}^+$  ions react with hydrogen peroxide ( $\text{H}_2\text{O}_2$ ) to produce hydroxyl radicals, which break down the peptidoglycan layer. Following this,  $\text{Cu}^+$  ions enter the periplasmic space, separating the cytosol from the plasma membrane, which leads to membrane damage. Some  $\text{Cu}^+$  ions penetrate the cell and catalyze the formation of reactive oxygen species (ROS), which damage DNA and proteins. The pathway for this mechanism can be described as follows: (A)  $\rightarrow$  (B), (A)  $\rightarrow$  (B)  $\rightarrow$  (C)  $\rightarrow$  (D), or (A)  $\rightarrow$  (B)  $\rightarrow$  (C)  $\rightarrow$  (E).

The antibacterial effect of  $\text{Cu}_2\text{O}$  NPs also involves a photocatalytic reaction. Compared to Gram-positive bacteria, Gram-negative bacteria exhibit slight resistance to ROS, which may influence the antibacterial mechanisms in these bacteria. Therefore, the specific mechanism(s) responsible for the antibacterial effects of Cu may vary between Gram-positive and Gram-negative bacteria. However, it remains unclear whether a single mechanism or a combination of mechanisms is responsible for the overall antibacterial effect.

*C. albicans*, a dimorphic fungus, can cause several infections, ranging from mild, superficial cutaneous infections to severe invasive candidiasis, which may lead to disability and mortality in immunocompromised patients. As shown in Fig. 6(f) and (i), we observed circular, white cells of *C. albicans*. White cells are epigenetically distinct from opaque cells, and although they are less efficient at mating, they have been shown to cause more virulent systemic infections.<sup>70,71</sup>

The mechanism by which  $\text{Cu}_2\text{O}$  NP-PP meltblown nonwoven fabrics inhibit the growth of *C. albicans* is as follows: the nonwoven textile prepared using the  $\text{Cu}_2\text{O}$  NP-embedded PP masterbatches releases  $\text{Cu}^+$  ions, which trigger the production of significant amounts of reactive oxygen species (ROS) in *C. albicans* through Fenton-like reactions. In the presence of  $\text{H}_2\text{O}_2$ ,

$\text{Cu}^+$  ions oxidize various cellular substrates, causing cellular damage in a typical Fenton-like reaction, similar to the behavior of iron.<sup>72</sup> Moreover, the level of membrane damage induced by  $\text{Cu}^+$  ions was significantly higher than that caused by  $\text{Cu}^{2+}$  ions. This can be attributed to the fact that  $\text{Cu}_2\text{O}$  NP-PP meltblown nonwoven fabrics continue to release  $\text{Cu}^+$  ions over time after contact with *C. albicans*. The high positive surface charge of  $\text{Cu}^+$  ions may contribute to membrane damage. Given that *C. albicans* cells are electronegative, their cell walls can effectively bind with positively charged inorganic ions, potentially facilitating electrostatic interactions with  $\text{Cu}^+$  ions. This interaction may play a significant role in the cellular damage of *C. albicans*.<sup>73</sup>

The antibacterial effect of noble metals on Gram-positive and Gram-negative bacteria varies due to differences in their cell morphology. A recent study showed that  $\text{Cu}_2\text{O}$  NPs are more effective against Gram-positive bacteria than Gram-negative bacteria, which can be attributed to the differences in their cell wall structures. Gram-negative bacteria have a three-layered cell envelope, with a thick outer membrane that acts as a barrier to reactive oxygen species (ROS) generated through the Fenton reaction. Ren *et al.* observed that  $\text{Cu}^+$  ions exhibited stronger antibacterial activity against *S. aureus* compared to *E. coli*. They attributed this result to the higher isoelectric point of the membranes of Gram-positive bacteria at the same pH, which creates a more negatively charged surface. This enhanced negative charge facilitates stronger interaction with metallic ions, thereby more effectively inhibiting *S. aureus*.<sup>74,75</sup>

Table 1 summarizes the antibacterial activity of the fabrics prepared using  $\text{Cu}_2\text{O}$  NP-embedded PP masterbatches against the selected bacteria and fungus. The  $\text{Cu}_2\text{O}$  NP-PP meltblown nonwoven fabric exhibited an antibacterial activity value of 5.21 against *Escherichia coli* after 18–24 h of contact, as shown in





**Table 1** Antimicrobial activities of Cu<sub>2</sub>O NP-PP meltblown nonwoven fabrics at the contact times of 18–24 h

Bacteria species	Antimicrobial activity (As-fabricated)	Antimicrobial activity (One year later)
<i>P. aeruginosa</i> (ATCC 10145)	5.24	5.19
<i>E. coli</i> (ATCC 8739)	5.21	5.15
MRSA (ATCC 33591)	5.33	5.27
<i>K. pneumonia</i> (ATCC 4352)	5.57	5.51
<i>S. aureus</i> (ATCC 6538P)	5.86	5.79
<i>C. albicans</i> (ATCC 10231)	5.38	5.32

Table 1 and Table S2 (ESI<sup>†</sup>). Additionally, all the activity values were in the range of 5–6, indicating that the Cu<sub>2</sub>O NP-PP meltblown nonwoven fabrics demonstrated excellent antimicrobial activity against all the selected microorganisms. Our results showed no significant difference in the effectiveness of the Cu<sub>2</sub>O NP-PP meltblown nonwoven fabrics against Gram-positive and Gram-negative bacteria after 18–24 h of contact. The similar effectiveness against both types of bacteria can be attributed to the relatively long contact time used in our experiments compared to previous studies. To further test our hypothesis, we examined the antibacterial activity of the Cu<sub>2</sub>O NP-PP meltblown nonwoven fabrics against *S. aureus*, *E. coli*, and *P. aeruginosa* with contact times of 1, 2, and 4 h. As shown in Fig. S7 (ESI<sup>†</sup>), the Cu<sub>2</sub>O NP-PP meltblown nonwoven fabrics more effectively inhibited *S. aureus* than *E. coli* and *P. aeruginosa* when the contact time was under 2 h. Significant antimicrobial activity was observed against *S. aureus*, but not against the other bacteria within the first 2 h. This could be because the cell membrane of Gram-positive bacteria is thinner than that of Gram-negative bacteria, allowing Cu<sup>+</sup> ions to penetrate more easily without causing immediate damage. Subsequently, Cu<sup>+</sup> ions catalyze the formation of ROS, which damages the DNA of the cell. The antimicrobial mechanism follows path (a) → (b) or (a) → (c), as shown in Fig. 8. However, Cu<sup>+</sup> ions require more time to penetrate and damage the cell membrane of Gram-negative bacteria, which have a more complex, three-layered cell envelope. Our results suggest that Gram-negative bacteria exhibit stronger resistance to Cu<sub>2</sub>O NPs during shorter contact times. Furthermore, we tested the antibacterial activity of the Cu<sub>2</sub>O NP-PP melt-blown nonwoven fabric after 12 months of storage. The results showed that the antibacterial activity slightly decreased compared to the freshly prepared Cu<sub>2</sub>O NP-PP melt-blown nonwoven fabric. However, the antibacterial activity remained above 5, indicating that the fabric still exhibited good antibacterial properties after one year. The main reason for this result is that we embedded the Cu<sub>2</sub>O NPs into the PP polymer, which protected the Cu<sub>2</sub>O NPs from environmental factors and prevented their oxidation. The detail parameters are shown in Table S3 (ESI<sup>†</sup>). These results are generally consistent with the XPS result, as shown in Fig. S5 (ESI<sup>†</sup>).

The relatively longer time required for effective antimicrobial activity against Gram-negative bacteria, compared to Gram-positive bacteria can be attributed to several factors. In addition

to the thicker cell membrane of Gram-negative bacteria, the surface of the Cu<sub>2</sub>O NP-PP meltblown nonwoven fabrics was found to be electrostatically neutral, as shown by the zeta potential measurements. As a result, the nonwoven fabric prepared with the Cu<sub>2</sub>O NP-embedded PP masterbatches did not exhibit immediate antimicrobial activity upon direct contact with bacteria. However, after a certain period of contact, the fabric could release copper or cuprous ions. The interaction of these positively charged ions with the negatively charged bacterial surface could inhibit bacterial growth. The primary antimicrobial mechanism for long contact times with Gram-negative bacteria follows path (A) → (B) → (C) → (D), or (A) → (B) → (C) → (E). The antimicrobial mechanism for Gram-positive bacteria is similar but occurs along paths (A) → (B) → (C) → (b) and (A) → (B) → (C) → (c). Thus, to enhance the antimicrobial activity against Gram-negative bacteria, the concentration of Cu<sub>2</sub>O NPs in the fabric should be increased in future applications.

Washing resistance is crucial for the commercialization of antimicrobial textiles using noble metals as antimicrobial agents. However, the coating processes commonly used in the textile industry, such as spraying and dipping, weakly bond Cu to fabrics. Additionally, these post-processing methods generate a large amount of wastewater, which is harmful to the environment. Furthermore, another approach, which involves using bridging agents to improve the Cu-fabric affinity, may not be universally applicable to all types of fibers. In contrast, our approach, where Cu<sub>2</sub>O NPs are directly embedded into masterbatches, provides satisfactory washing resistance for antimicrobial textiles. This method can be applied not only to PP but also PET, a fiber widely used in functional textiles. The results showed that the antimicrobial activity against *E. coli* decreased by only 3.8% after 50 washes. Moreover, the antimicrobial activity against all the tested bacteria remained above 94%, as shown in Table 2 and Table S4 (ESI<sup>†</sup>). These results for *E. coli* are more favorable than the reductions observed in previous studies, such as a 5% reduction after 50 washes for AgNP@HTCS antibacterial fabrics, 25% reduction after 10 washes for surfactants stabilizing CuO-NPs on fiber surfaces, 2% reduction after 10 washes for improving the adhesion properties of CuO-NPs on cotton fibers using a non-toxic, biocompatible starch material (with a 7.7% reduction in *S. aureus*), and 26.4% reduction after 25 washes for Cu<sub>2</sub>O fabrics.<sup>76–79</sup>

**Table 2** Washing resistance of antimicrobial activities of Cu<sub>2</sub>O NP-PET meltblown nonwoven fabrics

Bacteria species	Antimicrobial activity		
	Before washes	After washes	Reduction (%)
<i>P. aeruginosa</i> (ATCC 10145)	5.77	5.43	94.1
<i>E. coli</i> (ATCC 8739)	5.77	5.55	96.2
MRSA (ATCC 33591)	5.83	5.59	95.9
<i>K. pneumonia</i> (ATCC 4352)	5.86	5.55	94.7
<i>S. aureus</i> (ATCC 6538P)	5.62	5.42	96.4



The antimicrobial activity was categorized as very effective according to JIS L 1902:2015. Thus, our results demonstrate that our approach can solve the problem of antimicrobial durability in textiles. The COVID-19 pandemic has caused widespread morbidity and mortality globally, disrupting economies and lifestyles. The SARS-CoV-2 virus, which causes COVID-19, can remain viable on some solid surfaces for up to a week.<sup>80,81</sup> Therefore, mechanisms for reducing the viability of SARS-CoV-2 on surfaces are urgently needed. Our study, along with previous research, suggests that Cu<sub>2</sub>O-based polymer nanocomposites can reduce the viability of bacteria and viruses.<sup>82</sup> Consequently, the Cu<sub>2</sub>O NP-embedded PP and PET masterbatches developed in this study can be applied for the production of face masks, surgical masks, and high-efficiency particulate air (HEPA) filters used in hospitals. These Cu<sub>2</sub>O NP-embedded masks and filters can reduce the viability of viruses and improve the efficacy of medical treatments.

## Conclusions

This study described an innovative method of doping Cu<sub>2</sub>O NPs into masterbatches to manufacture Cu<sub>2</sub>O NP-embedded textiles that showed excellent antimicrobial activity. When the contact time was in the range of 18–24 h, the antimicrobial activity of the Cu<sub>2</sub>O NP-embedded PP textiles showed their effectiveness in inhibiting Gram-positive and Gram-negative bacteria. The textiles made from these masterbatches could effectively eliminate copper-green *Pseudomonas*, *Escherichia coli*, MRSA, *Klebsiella pneumoniae*, *Staphylococcus aureus*, and *Candida albicans*, even after being stored for a long period or washed 50 times, demonstrating long-lasting antibacterial activity. In terms of application, we demonstrated that the Cu<sub>2</sub>O NP-embedded PP masterbatches can be used to manufacture antibacterial masks and similar products. We also successfully embedded Cu<sub>2</sub>O NP into PET, which can potentially be used in medical textiles in the future, such as surgical gowns, hospital bed sheets, and air filters, to reduce hospital-acquired infections.

## Abbreviations

PET	Polyethylene terephthalate
HAIs	Healthcare-associated infections
MRSA	Methicillin-resistant <i>Staphylococcus aureus</i>
VRE	Vancomycin-resistant <i>Enterococcus</i>
ROS	Reactive oxygen species
Cu NPs	Copper nanoparticles
PP	Polypropylene
Cu <sub>2</sub> O	Cuprous oxide
DLS	Dynamic light scattering
CuO	Copper oxide
Cu-PP	Cu-embedded PP
SEM	Scanning electron microscopy
EDS	Energy dispersive spectroscopy
TGA	Thermogravimetric analysis
XRD	X-Ray diffraction

XPS	X-Ray photoelectron spectroscopy
CFU per mL	Colony forming unit per milliliter
JIS	Japanese Industrial Standard
JTETC	Japan Textile Evaluation Technology Council
PS	Polystyrene
AATCC	American Association of Textile Chemists and Colorists
HEPA	High-efficiency particulate air filter

## Author contributions

The manuscript was written through contributions of all authors. All authors have given approval to the final version of the manuscript.

## Data availability

Data are not available for sharing. The raw/processed data required to reproduce the above findings cannot be shared at this time as the data also form part of an ongoing study.

## Conflicts of interest

The authors declare no competing financial interest.

## Acknowledgements

The authors acknowledge the financial support of the National Science and Technology Council (NSTC 113-2221-E-143-003-, NSTC 113-2622-E-143-001-, NSTC 111-2628-E-143-001-MY2). The author expresses gratitude to Dr. Yi-Chung Wang for his guidance in the fabrication of Cu<sub>2</sub>O NP-based antimicrobial textiles. The authors also thank Mytrex Health Technology for their technical support in meltblown nonwoven textiles. Additionally, they gratefully acknowledge Yuang Shen Company for their valuable discussions on masterbatch fabrication. Finally, the authors gratefully acknowledge the use of a high-resolution scanning electron microscope equipment (Hitachi SU8000, EM003600) belonging to the Core Facility Center of National Cheng Kung University.

## References

- 1 D. Q. Balbas, G. Lanterna, C. Cirrincione, R. Fontana and J. Striova, Non-invasive identification of textile fibres using near-infrared fibre optics reflectance spectroscopy and multivariate classification techniques, *Eur. Phys. J. Plus*, 2022, **137**, 85.
- 2 A. Libanori, G. Chen, X. Zhao, Y. Zhou and J. Chen, Smart textiles for personalized healthcare, *Nat. Electron.*, 2022, **5**, 142–156.
- 3 S. Mollick, M. R. Repon, A. Haji, M. A. Jalil, T. Islam and M. M. Khan, Progress in self-cleaning textiles: parameters, mechanism and applications, *Cellulose*, 2023, **30**, 10633–10680.





- 4 D. Li, S. Feng, J. Tao, S. Yu, Y. He, R. Yu, H. Xiang, C. Wang and M. Zhu, Optimizing Sustainability in Textile Recycling: Life Cycle Assessment of Recycled Polyester Staple Fibers with a Focus on Carbon Emissions, Energy Efficiency, and Water Conservation, *ACS Sustainable Chem. Eng.*, 2024, **12**, 17347–17356.
- 5 J. Fu, T. Liu, S. S. B. Touhid, F. Fu and X. Liu, Functional Textile Materials for Blocking COVID-19 Transmission, *ACS Nano*, 2023, **17**, 1739–1763.
- 6 L. Windler, M. Height and B. Nowack, Comparative Evaluation of Antimicrobials for Textile Applications, *Environ. Int.*, 2013, **53**, 62–73.
- 7 M. Vincent, P. Hartemann and M. Engels-Deutsch, Antimicrobial Applications of Copper, *Int. J. Hyg. Environ. Health*, 2016, **219**(7), 585–591.
- 8 C. D. Sifri, G. H. Burke and K. B. Enfield, Reduced Health Care-Associated Infections in an Acute Care Community Hospital Using a Combination of Self-Disinfecting Copper-Impregnated Composite Hard Surfaces and Linens, *Am. J. Infect. Control*, 2016, **44**(12), 1565–1571.
- 9 E. L. Marcus, H. Yosef, G. Borkow, Y. Caine, A. Sasson and A. E. Moses, Reduction of Health Care-Associated Infection Indicators by Copper Oxide-Impregnated Textiles: Crossover, Double-Blind Controlled Study in Chronic Ventilator-Dependent Patients, *Am. J. Infect. Control*, 2017, **45**(4), 401–403.
- 10 N. van Doremalen, T. Bushmaker, D. H. Morris, M. G. Holbrook, A. Gamble, B. N. Williamson, A. Tamin, J. L. Harcourt, N. J. Thornburg and S. I. Gerber, Aerosol and Surface Stability of SARS-CoV-2 as Compared with SARS-CoV-1, *N. Engl. J. Med.*, 2020, **382**(16), 1564–1567.
- 11 S. U. Islam, B. S. Butola and F. Mohammad, Silver nanomaterials as future colorants and potential antimicrobial agents for natural and synthetic textile materials, *RSC Adv.*, 2016, **6**, 44232–44247.
- 12 M. M. Hossain, T. Islam, M. A. Jalil, S. M. Rakibuzzaman, S. M. Surid, M. R. I. Zayed, A. Talukder and S. Hossain, Advancements of eco-friendly natural antimicrobial agent and their transformative role in sustainable textiles, *SPE Polym.*, 2024, **5**, 241–276.
- 13 V. O. Veselova, V. A. Plyuta, A. N. Kostrov, D. N. Vtyurina, V. O. Abramov, A. V. Abramova, Y. I. Voitov, D. A. Padiy, V. T. H. Thu, L. T. Hue, D. T. T. Trang, A. E. Baranchikov, I. A. Khmel, V. A. Nadtochenko and V. K. Ivanov, Long-Term Antimicrobial Performance of Textiles Coated with ZnO and TiO<sub>2</sub> Nanoparticles in a Tropical Climate, *J. Funct. Biomater.*, 2022, **13**, 233.
- 14 R. Gulati, S. Sharma and R. K. Sharma, Antimicrobial textile: recent developments and functional perspective, *Polym. Bull.*, 2022, **79**, 5747–5771.
- 15 F. Quartinello, C. Tallian, J. Auer, H. Schön, R. Vielnascher, S. Weinberger, K. Wieland, A. M. Weihs, Al. H. Rollett, B. Lendl, A. H. Teuschl, A. Pellis and G. M. Guebitz, Smart textiles in wound care: functionalization of cotton/PET blends with antimicrobial nanocapsules, *J. Mater. Chem. B*, 2019, **7**, 6592–6603.
- 16 S. Andra, S. k Balu, J. Jeevanandam and M. Muthalagu, Emerging nanomaterials for antibacterial textile fabrication, *Naunyn-Schmiedeberg's Arch. Pharmacol.*, 2021, **394**, 1355–1382.
- 17 Y. Xia, X. Ma, J. Gao, G. Chen, Z. Li, X. Wu, Z. Yu, J. Xing, L. Sun and H. Ruan, *et al.*, A Flexible Caterpillar-Like Gold Nanoparticle Assemblies with Ultrasmall Nanogaps for Enhanced Dual-Modal Imaging and Photothermal Therapy, *Small*, 2018, **14**(19), 1800094.
- 18 P. Ganguli and S. Chaudhuri, Nanomaterials in antimicrobial paints and coatings to prevent biodegradation of man-made surfaces: A review, *Mater. Today: Proc.*, 2021, **45**, 3769–3777.
- 19 H. A. Reyes, S. Moreno, I. P. López, M. A. Vera, L. Patrón-Romero, B. Borrego, A. R. Escamilla, V. M. Daniel, A. Brun and N. Bogdanchikova, Evaluation of silver nanoparticles for the prevention of SARS-CoV-2 infection in health workers: *In vitro* and *in vivo*, *PLoS One*, 2021, **16**(8), e0256401.
- 20 I. Osório, R. Igreja, R. Franco and J. Cortez, Incorporation of Silver Nanoparticles on Textile Materials by an Aqueous Procedure, *Mater. Lett.*, 2012, **75**, 200–203.
- 21 J. Pulit-Prociak, J. Chwastowski, A. Kucharski and M. Banach, Functionalization of Textiles with Silver and Zinc Oxide Nanoparticles, *Appl. Surf. Sci.*, 2016, **385**, 543–553.
- 22 M. Guzman, J. Dille and S. Godet, Synthesis and Antibacterial Activity of Silver Nanoparticles against Gram-positive and Gram-negative Bacteria, *Nanomed. Nanotechnol.*, 2012, **8**(1), 37–45.
- 23 L. Tamayo, M. Azócar, M. Kogan, A. Riveros and M. Páez, Copper-Polymer Nanocomposites: An Excellent and Cost-Effective Biocide for Use on Antibacterial Surfaces, *Mater. Sci. Eng., C*, 2016, **69**, 1391–1409.
- 24 N. Jayarambabu, A. Akshaykranth, T. Venkatappa Rao, K. Venkateswara Rao and R. Rakesh Kumar, Green Synthesis of Cu Nanoparticles Using Curcuma Longa Extract and Their Application in Antimicrobial Activity, *Mater. Lett.*, 2020, **259**, 126813.
- 25 A. Lazary, I. Weinberg, J. J. Vatine, A. Jefidoff, R. Bardenstein, G. Borkow and N. Ohana, Reduction of Healthcare-Associated Infections in a Long-Term Care Brain Injury Ward by Replacing Regular Linens with Biocidal Copper Oxide Impregnated Linens, *Int. J. Infect. Dis.*, 2014, **24**, 23–29.
- 26 B. Saeed, C. Alex, H. Mohsen, P. Leo and A. D. William, A Surface Coating that Rapidly Inactivates SARS-CoV-2, *ACS Appl. Mater. Interfaces*, 2020, **12**, 34487–35766.
- 27 G. Borkow, Safety of Using Copper Oxide in Medical Devices and Consumer Products, *Curr. Chem. Biol.*, 2012, **6**, 86–92.
- 28 C. Yang, R. Jiana, K. Huang, Q. Wang and B. Feng, Antibacterial mechanism for inactivation of E. Coli by AgNPs@polydoamine/titania nanotubes via speciation analysis of silver ions and silver nanoparticles by cation exchange reaction, *Microchem. J.*, 2021, **160**, 105636.
- 29 B. Jia, Y. Mei, L. Cheng, J. Zhou and L. Zhang, Preparation of Copper Nanoparticles Coated Cellulose Films with Antibacterial Properties through One-Step Reduction, *ACS Appl. Mater. Interfaces*, 2012, **4**(6), 2897–2902.



- 30 N. C. Cady, J. L. Behnke and A. D. Strickland, Copper-Based Nanostructured Coatings on Natural Cellulose: Nanocomposites Exhibiting Rapid and Efficient Inhibition of a Multi-Drug Resistant Wound Pathogen, *A. Baumannii*, and Mammalian Cell Biocompatibility *In Vitro*, *Adv. Funct. Mater.*, 2011, **21**(13), 2506–2514.
- 31 J. Xiao, S. Chen, J. Yi, H. F. Zhang and G. A. Ameer, A Cooperative Copper Metal–Organic Framework–Hydrogel System Improves Wound Healing in Diabetes, *Adv. Funct. Mater.*, 2016, **27**(1), 1604872.
- 32 X. Ren, C. Yang, L. Zhang, S. Li, S. Shi, R. Wang, X. Zhang, T. Yue, J. Sun and J. Wang, Copper Metal–Organic Frameworks Loaded on Chitosan Film for the Efficient Inhibition of Bacteria and Local Infection Therapy, *Nanoscale*, 2019, **11**(24), 11830–11838.
- 33 J. R. Morones-Ramirez, J. A. Winkler, C. S. Spina and J. J. Collins, Silver Enhances Antibiotic Activity Against Gram-negative Bacteria, *Sci. Transl. Med.*, 2013, **5**(190), 190ra81.
- 34 K. San, J. Long, C. A. Michels and N. Gadura, Antimicrobial Copper Alloy Surfaces Are Effective against Vegetative but Not Sporulated Cells of Gram-positive *Bacillus Subtilis*, *MicrobiologyOpen*, 2015, **4**(5), 753–763.
- 35 R. Z. Javiera, B. Nicolás and M. P. D. José, Toxicity Mechanisms of Copper Nanoparticles and Copper Surfaces on Bacterial Cells and Viruses, *Int. J. Mol. Sci.*, 2023, **24**, 10503.
- 36 A. K. Chatterjee, R. Chakraborty and T. Basu, Mechanism of Antibacterial Activity of Copper Nanoparticles, *Nanotechnology*, 2014, **25**(13), 135101.
- 37 L. Macomber and J. A. Imlay, The Iron–Sulfur Clusters of Dehydratases Are Primary Intracellular Targets of Copper Toxicity, *Proc. Natl. Acad. Sci. U. S. A.*, 2009, **106**(20), 8344–8349.
- 38 I. Elchennawi and S. O. Choudens, Iron–Sulfur Clusters toward Stresses: Implication for Understanding and Fighting Tuberculosis, *Inorganics*, 2022, **10**, 174.
- 39 Y. Liu and J. A. Imlay, Cell Death from Antibiotics Without the Involvement of Reactive Oxygen Species, *Science*, 2013, **339**(6124), 1210–1213.
- 40 I. Keren, Y. Wu, J. Inocencio, L. R. Mulcahy and K. Lewis, Killing by Bactericidal Antibiotics Does Not Depend on Reactive Oxygen Species, *Science*, 2013, **339**(6124), 1213–1216.
- 41 H. E. Emama and T. Bechtold, Cotton fabrics with UV blocking properties through metal salts deposition, *Appl. Surf. Sci.*, 2015, **357**, 1878–1889.
- 42 A. Errokh, W. Cheikhrouhou, A. M. Ferraria, A. M. Botelho do Rego and S. Boufi, Cotton decorated with Cu<sub>2</sub>O–Ag and Cu<sub>2</sub>O–Ag–AgBr NPs *via* an *in situ* sacrificial template approach and their antibacterial efficiency, *Colloids Surf., B*, 2021, **200**, 111600.
- 43 A. A. Hassabo, E. I. Ibrahim, B. A. Ali and H. E. Emam, Anticancer effects of biosynthesized Cu<sub>2</sub>O nanoparticles using marine yeast, *Biocatal. Agric. Biotechnol.*, 2022, **39**, 102261.
- 44 H. E. Emama and T. Bechtold, Cotton fabrics with UV blocking properties through metal salts, *Appl. Surf. Sci.*, 2015, **357**, 1878–1889.
- 45 C. Sun, Y. Li, Z. Li, Q. Su, Y. Wang and X. Liu, Durable and Washable Antibacterial Copper Nanoparticles Bridged by Surface Grafting Polymer Brushes on Cotton and Polymeric Materials, *J. Nanomater.*, 2018, 6546193.
- 46 W. Fan, Y. Zhang, W. Wang, Y. Sun, K. Dong, S. Wang, C. Zhang and X. Yu, Durable antibacterial and temperature regulated core-spun yarns for textile health and comfort applications, *Chem. Eng. J.*, 2023, **455**, 140917.
- 47 R. Suna, D. Liu, X. Tian, Q. Zuo, D. Wang and S. Wen, The role of copper ion and soluble starch used as a combined depressant in the flotation separation of fluorite from calcite: New insights on the application of modified starch in mineral processing, *Miner. Eng.*, 2022, **181**, 107550.
- 48 D. J. da Silva, A. G. Souza, P. H. Camani and D. S. Rosa, Bactericidal Properties of Natural Fibers Hybrid Functionalized with ZnO/Cu<sup>2+</sup> and ZnO/Cu<sup>0</sup>, *Fibers Polym.*, 2023, **24**, 959–973.
- 49 H. B. Ahmed, N. S. El-Hawary, H. M. Mashaly and H. E. Emam, End-to-End surface manipulation of dyed silk for perfection of coloration, UV-resistance and biocidal performance, *J. Mol. Struct.*, 2024, **1305**, 137766.
- 50 A. Mahdy, M. G. Mohamed, K. I. Aly, H. B. Ahmed and H. E. Emam, Liquid crystalline polybenzoxazines for manufacturing of technical textiles: Water repellency and ultraviolet shielding, *Polym. Test.*, 2023, **119**, 107933.
- 51 H. E. Emam, S. Zaghloul and H. B. Ahmed, Full ultraviolet shielding potency of highly durable cotton *via* self-implantation of palladium nanoclusters, *Cellulose*, 2022, **29**, 4787–4804.
- 52 H. E. Emam, M. E. Shahat, M. S. Hasanin and H. B. Ahmed, Potential military cotton textiles composed of carbon quantum dots clustered from 4-(2,4-dichlorophenyl)-6-oxo-2-thioxohexahydropyrimidine-5-carbonitrile, *Cellulose*, 2021, **28**, 9991–10011.
- 53 H. B. Ahmed, K. M. Abualnaja, R. Y. Gharee, A. A. Ibrahim, N. R. Abdelsalam and H. E. Emame, Technical textiles modified with immobilized carbon dots synthesized with infrared assistance, *J. Colloid Interface Sci.*, 2021, **604**, 15–29.
- 54 H. E. Emam, R. M. Abdelhameed and H. B. Ahmed, Multi-finished protective viscose textile *via* infrared assistedonepot incorporation of Ce-organic framework, *Cellulose*, 2024, **31**, 7015–7030.
- 55 H. E. Emam, N. S. El-Hawary, H. M. Mashaly and H. B. Ahmed, Involvement of silver and palladium with red peanuts skin extract for cotton functionalization, *Sci. Rep.*, 2023, **13**, 16131.
- 56 H. E. Emam, T. Hamouda, E. A. M. Emam, O. M. Darwesh and H. B. Ahmed, Nano-scaled polyacrylonitrile for industrialization of nanofibers with photoluminescence and microbicide performance, *Sci. Rep.*, 2024, **14**, 7926.
- 57 T. Chang, R. P. Babu, W. Zhao, C. M. Johnson, P. Hedström, I. Odnevall and C. Leygraf, High-Resolution Microscopical Studies of Contact Killing Mechanisms on Copper-Based Surfaces, *ACS Appl. Mater. Interfaces*, 2021, **13**, 49402–49413.
- 58 S. Behzadinasab, M. Hosseini, M. D. Williams, H. M. Ivester, I. C. Allen, J. O. Falkinham III and W. A. Ducker,





- Antimicrobial activity of cuprous oxide-coated and cupric oxide-coated surfaces, *J. Hosp. Infect.*, 2022, **129**, 58–64.
- 59 R. Pachaiappan, S. Rajendran, P. L. Show, K. Manavalan and M. Naushad, Metal/metal oxide nanocomposites for bactericidal effect: A review, *Chemosphere*, 2021, **272**, 128607.
  - 60 S. Mori and H. Okamoto, A unified theory of determining the electrophoretic velocity of mineral particles in the rectangular micro-electrophoresis cell, *Fusen*, 1980, **27**, 117–126.
  - 61 V. Smoluchowski, *Handbuch der Elektrizität und des Magnetismus*, 2. Leipzig, Germany, Barth, 1921, p. 366.
  - 62 S. N. Ariffin, H. N. Lim, F. A. Jumeri, M. Zobir, A. H. Abdullah, M. Ahmad, N. A. Ibrahim, N. M. Huang, P. S. Teo, K. Muthoosamy and I. Harrison, Modification of polypropylene filter with metal oxide and reduced graphene oxide for water treatment, *Ceram. Int.*, 2014, **40**, 6927–6936.
  - 63 M. Endo-Kimura, K. Wang, Z. Bielan, M. Janczarek, A. Markowska-Szczupak and E. Kowalsk, Antibacterial activity of core-shell  $\text{Cu}_x\text{O}/\text{TiO}_2$  photocatalyst under UV, vis and dark, *Surf. Interfaces*, 2022, **32**, 102125.
  - 64 L. A. Tamayo, P. A. Zapata, F. M. Rabagliati, M. I. Azócar, L. A. Muñoz, X. Zhou, G. E. Thompson and M. A. Páez, Antibacterial and Non-Cytotoxic Effect of Nanocomposites Based in Polyethylene and Copper Nanoparticles, *J. Mater. Sci.: Mater. Med.*, 2015, **26**(3), 129.
  - 65 P. S. Kumar, J. Johnson and C. S. Biju, Structural, morphological, and optoelectronic characteristics of Zn, Cd-codoped CuO nanostructures, *J. Mater. Sci.: Mater. Electron.*, 2024, **35**, 1233.
  - 66 Z. Dan, Y. Yang, F. Qin, H. Wang and H. Chang, Facile Fabrication of  $\text{Cu}_2\text{O}$  Nanobelts in Ethanol on Nanoporous Cu and Their Photodegradation of Methyl Orange, *Materials*, 2018, **11**, 446.
  - 67 M. C. Biesinger, Advanced analysis of copper X-ray photoelectron spectra, *Surf. Interface Anal.*, 2017, **49**, 1325–1334.
  - 68 D. R. Soll, White-opaque switching in *Candida albicans*: cell biology, regulation, and function, *Microbiol. Mol. Biol. Rev.*, 2024, **88**(2), e0004322.
  - 69 M. G. Miller and A. D. Johnson, White-opaque switching in *Candida albicans* is controlled by mating-type locus homeodomain proteins and allows efficient mating, *Cell*, 2002, **110**, 293–302.
  - 70 C. C. Winterbourn, Toxicity of iron and hydrogen peroxide: the Fenton reaction, *Toxicol. Lett.*, 1995, **82–83**, 969–974.
  - 71 A. R. Padmavathi, S. Murthy P, A. Das, A. Priya, T. J. Sushmitha, S. K. Pandian and S. R. Toleti, Impediment to growth and yeast-to-hyphae transition in *Candida albicans* by copper oxide nanoparticles, *Biofouling*, 2020, **36**(1), 56–72.
  - 72 J. Niu, Y. Sun, F. Wang, C. Zhao, J. Ren and X. Qu, Photo-modulated Nanozyme Used for a Gram-Selective Antimicrobial, *Chem. Mater.*, 2018, **30**(20), 7027–7033.
  - 73 C. Wang, X. Qian and X. An, *In Situ* Green Preparation and Antibacterial Activity of Copper-Based Metal–Organic Frameworks/Cellulose Fibers (HKUST-1/CF) Composite, *Cellulose*, 2015, **22**(6), 3789–3797.
  - 74 S. Nam, B. D. Condon, C. D. Delhom and K. R. Fontenot, Silver-cotton nanocomposites: nano-design of microfibrillar structure causes morphological changes and increased tenacity, *Sci. Rep.*, 2016, **6**, 37320.
  - 75 R. Hasan, Production of Antimicrobial Textiles by Using Copper Oxide Nanoparticle, *Int. J. Contemp. Res. Rev.*, 2018, **09**, 20195–20202.
  - 76 Z. Liu, L. Wang, X. Zhao, Y. Luo, K. Zheng and M. Wu, Highly effective antibacterial AgNPs@hinokitiol grafted chitosan for construction of durable antibacterial fabrics, *Int. J. Biol. Macromol.*, 2022, **209**, 963–971.
  - 77 I. M. El-Nahhal, A. A. Elmanama, N. Amara, F. S. Qodih, M. Selmanec and M. M. Chehimi, The efficacy of surfactants in stabilizing coating of nano-structured CuO particles onto the surface of cotton fibers and their antimicrobial activity, *Mater. Chem. Phys.*, 2018, **215**, 221–228.
  - 78 I. M. El-Nahhal, J. Salem, F. S. Kodeh, A. Elmanama and R. Anbar, CuO-NPs, CuO-Ag nanocomposite and Cu(II)-curcumin complex coated cotton/starched cotton antimicrobial materials, *Mater. Chem. Phys.*, 2022, **285**, 126099.
  - 79 L. E. Román, C. Uribe, F. Paraguay-Delgado, J. G. Sutjianto, A. M. Navarrete-López, E. D. Gomez, J. L. Solís and M. M. Gómez, Physical and Surface Chemical Analysis of High-Quality Antimicrobial Cotton Fabrics Functionalized with  $\text{CuO}_x$  Grown *In Situ* from Different Copper Salts: Experimental and Theoretical Approach, *ACS Appl. Mater. Interfaces*, 2025, **17**, 1869–1882.
  - 80 S. Behzadinasab, A. Chin, M. Hosseini, L. Poon and W. A. Duc, A Surface Coating that Rapidly Inactivates SARS-CoV-2, *ACS Appl. Mater. Interfaces*, 2020, **12**, 34723–34727.
  - 81 S. Mori, T. Hara, K. Aso and H. Okamoto, Zeta Potential of Coal Fine-Particles in Aqueous Suspension, *Powder Technol.*, 1984, **40**, 161–165.
  - 82 A. Sze, D. Erickson, L. Ren and D. Li, Zeta-Potential Measurement Using the Smoluchowski Equation and the Slope of the Current–Time Relationship in Electroosmotic Flow, *J. Colloid Interface Sci.*, 2003, **261**(2), 402–410.

